Constraints on Carbon Monoxide Emissions Based on Tall Tower Measurements in the U.S. Upper Midwest

Su Youn Kim[1,2], Dylan B. Millet[1,*], Lu Hu[1], Michael J. Mohr[1], Tim J. Griffis[1], Deyong Wen[3], John C. Lin[4], Scot M. Miller[5], and Marcos Longo[5]

[1]University of Minnesota, St. Paul, MN 55108, USA

[2]Now at: Korea Institute of Science and Technology Evaluation and Planning, Seoul, South Korea

[3]University of Waterloo, Waterloo, ON N2L 3G1, Canada

[4]University of Utah, Salt Lake City, UT 84112, USA

[5]Harvard University, Cambridge, MA 02138, USA

* Correspondence to: Dylan B. Millet (dbm@umn.edu)

Supporting Information

S1. KCMP Tall Tower Measurements

We sample ambient air at 185 m height through a continuous 1.27 cm OD sampling line (PFA, Jensen Inert Products). The residence time for air in the line is approximately 2 minutes under normal sampling conditions. Carbon monoxide is measured at the KCMP tall tower every 3 minutes using gas chromatography (GC) with a reducing compound photometer (Peak Performer 1; Peak Laboratories LLC). In this technique, CO eluting from the GC column (Unibeads 1S and MS 13X) passes directly into a heated mercuric oxide bed (265°C). During the process, mercury vapor is liberated and subsequently measured by UV light absorption in the photometer cell. We carry out multi-point calibrations daily by dynamic dilution of a certified standard (Scott Specialty Gases; 10.1 ppm; stated accuracy ±2%) into home-made zero air

(Sofnocat catalyst bed maintained at 60°C). Calibrations span 0-350 ppb, which brackets the concentration range typically observed at the site. Under normal conditions, the R^2 values for 6-point calibration curves are > 0.999 for CO, with the relative standard deviation of residuals < 3%. The instrumental detection limit for CO is approximately 300 ppt.

S2. STILT Model Description

STILT computes the upstream influence on a measurement site by releasing a suite of particles from the receptor and following their transport backwards in time. Wind fields are provided by a mesoscale model, driven by meteorological reanalysis data, and interpolated to the explicit location of each particle. Turbulence is simulated by a Markov chain process. The evolution of particles backwards in time maps $I(\mathbf{x}_r, t_r \mid \mathbf{x}, t)$, reflecting the influence of a given location $(\mathbf{x}, t)$ in space and time on mixing ratios at the receptor (located at $\mathbf{x}_r$ and time t_r)[1]:

$$I\left(\mathbf{x}_r, t_r \big| \mathbf{x}, t\right) = \frac{\rho\left(\mathbf{x}_r, t_r \big| \mathbf{x}, t\right)}{N_{tot}}$$

(Equation 1)

where the density $\rho(\mathbf{x}_r, t_r \mid \mathbf{x}, t)$ of particles at $(\mathbf{x}, t)$ transported backwards in time from $(\mathbf{x}_r, t_r)$ is divided by the total number N_{tot} of particles released.

Accounting for the molar mass and density of air and the mixing height of emissions then yields the footprint function, $f(\mathbf{x}_r, t_r \mid x_i, y_j, t_m)$, which when coupled to a surface flux $F(x_i, y_j, t_m)$ quantifies the contribution of each location (x_i, y_j, t_m) in space and time to mixing ratios of an inert tracer at the receptor. Figure 2 in the main text shows the averaged footprint function at the KCMP tall tower for 2009 as derived by STILT.

STILT allows the user to specify the number of particles used in the simulation: a larger number provides improved statistics for computing the footprint, but at increased computational expense. For this work we carried out sensitivity runs using 100 and 1000 particles, for both

summer and winter, to evaluate the effect on simulated mixing ratios at the KCMP tall tower. A linear regression of CO mixing ratio between these simulations showed only minor differences (slope = 1.0; R = 0.95), and we therefore employ 100 particles in subsequent analyses. We also performed test simulations in which the particle trajectories were run 5 days versus 10 days backwards in time; again, these showed only minor differences and so 5-day back-trajectories were adopted for this work.

Boundary conditions, initial conditions, and photochemical production rates for CO are based on hourly output at 2° × 2.5° from the same GEOS-Chem simulation used to provide the OH fields. For the analyses in this paper we average the measured and simulated CO mixing ratios in two-hour intervals, and exclude convective periods as indicated by relevant indices from radiosonde data in Minneapolis (MSP, 44.85˚N, 93.57˚W): Lifted Index (LI) ≤ -4, Convective Available Potential Energy (CAPE) > 1500 J/kg, or K Index (KI) > 26.

We use three meteorological datasets to drive the STILT model and to assess the impact of transport uncertainty on our analysis: EDAS (Eta Data Assimilation System) and NARR (North American Regional Reanalysis) from the National Centers for Environmental Prediction (NCEP), and BRAMS (Brazilian developments on the Regional Atmospheric Modeling System)[2-4]. The horizontal domains of these three meteorological datasets are plotted in Figure S2. The EDAS data are archived at 3-hourly and 40 km horizontal resolution, while the NARR data are produced at 32 km horizontal resolution every 3 hours. The NARR system is similar to EDAS, except that it incorporates a number of additional data sets, uses a different cloud microphysics scheme, and employs a slightly finer horizontal resolution[4]. The BRAMS model originates from the Regional Atmospheric Modeling System (RAMS); a basic description is given by Freitas et al.[3]. The BRAMS runs employ a mass flux approach and the Mellor-Yamada

model for the cumulus scheme and eddy diffusion, respectively[5, 6]. The vertical coordinate is terrain-following with a resolution ranging from 150 m at the surface to 850 m at the top of the model domain. BRAMS was run at 15 km horizontal resolution over the domain shown in Figure S2 using 1° × 1° FNL analysis data provided by the NCEP Global Forecast System (GFS), with output saved hourly. In all cases, we set the floor for the nighttime mixing height in the model at 100 m, based on an analysis of nearby radiosonde data and a comparison between the measured and simulated diurnal cycles in CO.

S3. GEOS-Chem Model Description

GEOS-Chem (www.geos-chem.org) is a 3D CTM driven by GEOS-5.2 assimilated meteorological data from the NASA Global Modeling and Assimilation Office (GMAO). For this work, the model was configured as described by Millet et al.[7], with CO emissions over North America implemented as described for STILT. The model was run with 47 levels in the vertical extending up to 0.01 hPa. The 4° × 5° and 2° × 2.5° simulations were performed globally using 15 and 30 minute transport time steps, respectively. The 0.5° × 0.667° simulation was run over the nested domain shown in Figure S2 (10° to 70° N; 140° to 40°W) using a 10 minute transport time step, with lateral boundary conditions at each model layer based on 3-hourly output from the global 4° × 5° simulation. In all cases a 1-year spinup was used to remove any influence from initial conditions.

References

1.　　Lin, J. C.; Gerbig, C.; Wofsy, S. C.; Andrews, A. E.; Daube, B. C.; Davis, K. J.; Grainger, C. A., A near-field tool for simulating the upstream influence of atmospheric observations: The

Stochastic Time-Inverted Lagrangian Transport (STILT) model. *J. Geophys. Res.* **2003,** *108*, (D16), 4493, doi:10.1029/2002JD003161.

2.   Black, T. L., The new NMC mesoscale Eta Model: Description and forecast examples. *Weather Forecast.* **1994,** *9*, (2), 265-278.

3.   Freitas, S. R.; Longo, K. M.; Dias, M.; Chatfield, R.; Dias, P. S.; Artaxo, P.; Andreae, M. O.; Grell, G.; Rodrigues, L. F.; Fazenda, A.; Panetta, J., The Coupled Aerosol and Tracer Transport model to the Brazilian developments on the Regional Atmospheric Modeling System (CATT-BRAMS) - Part 1: Model description and evaluation. *Atmos. Chem. Phys.* **2009,** *9*, (8), 2843-2861.

4.   Mesinger, F.; DiMego, G.; Kalnay, E.; Mitchell, K.; Shafran, P. C.; Ebisuzaki, W.; Jovic, D.; Woollen, J.; Rogers, E.; Berbery, E. H.; Ek, M. B.; Fan, Y.; Grumbine, R.; Higgins, W.; Li, H.; Lin, Y.; Manikin, G.; Parrish, D.; Shi, W., North American Regional Reanalysis. *B. Am. Meteorol. Soc.* **2006,** *87*, (3), 343-360.

5.   Grell, G. A.; Devenyi, D., A generalized approach to parameterizing convection combining ensemble and data assimilation techniques. *Geophys. Res. Lett.* **2002,** *29*, (14), 1693, doi:10.1029/2002GL015311.

6.   Mellor, G. L.; Yamada, T., Development of a turbulence closure model for geophysical fluid problems. *Rev. Geophys.* **1982,** *20*, (4), 851-875.

7.   Millet, D. B.; Guenther, A.; Siegel, D. A.; Nelson, N. B.; Singh, H. B.; de Gouw, J. A.; Warneke, C.; Williams, J.; Eerdekens, G.; Sinha, V.; Karl, T.; Flocke, F.; Apel, E.; Riemer, D. D.; Palmer, P. I.; Barkley, M., Global atmospheric budget of acetaldehyde: 3D model analysis and constraints from in-situ and satellite observations. *Atmos. Chem. Phys.* **2010,** *10*, 3405-3425.
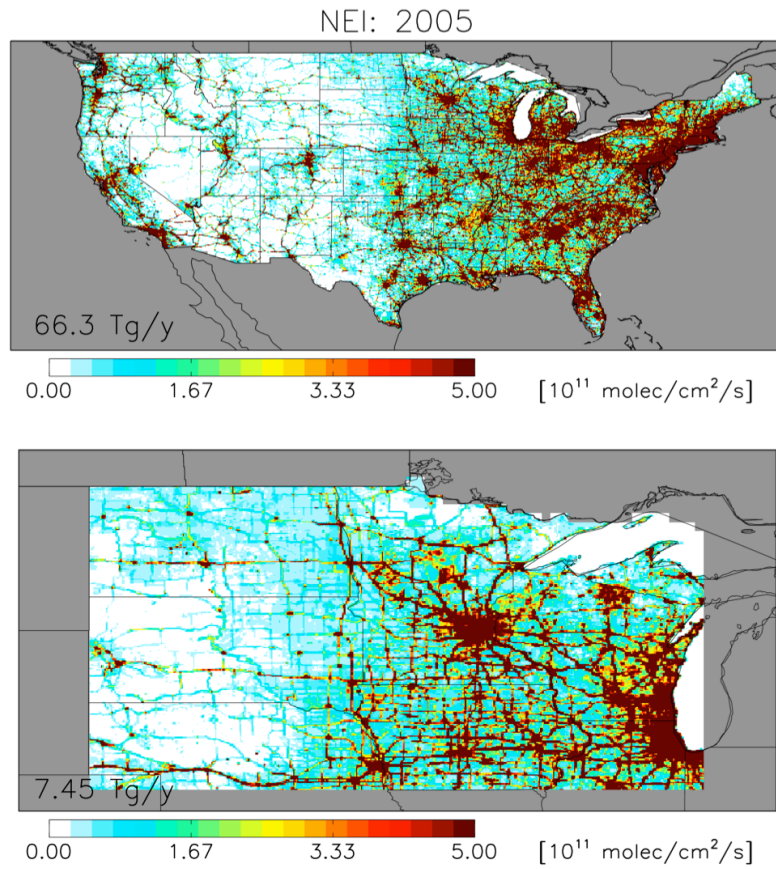
Figure S1. Annual anthropogenic surface CO emissions in the NEI 2005 emission inventory as implemented for the STILT simulations. Emissions shown are for year 2005 and gridded to 0.036° × 0.036°, and do not include fires. Numbers inset give the annual flux for the region plotted.
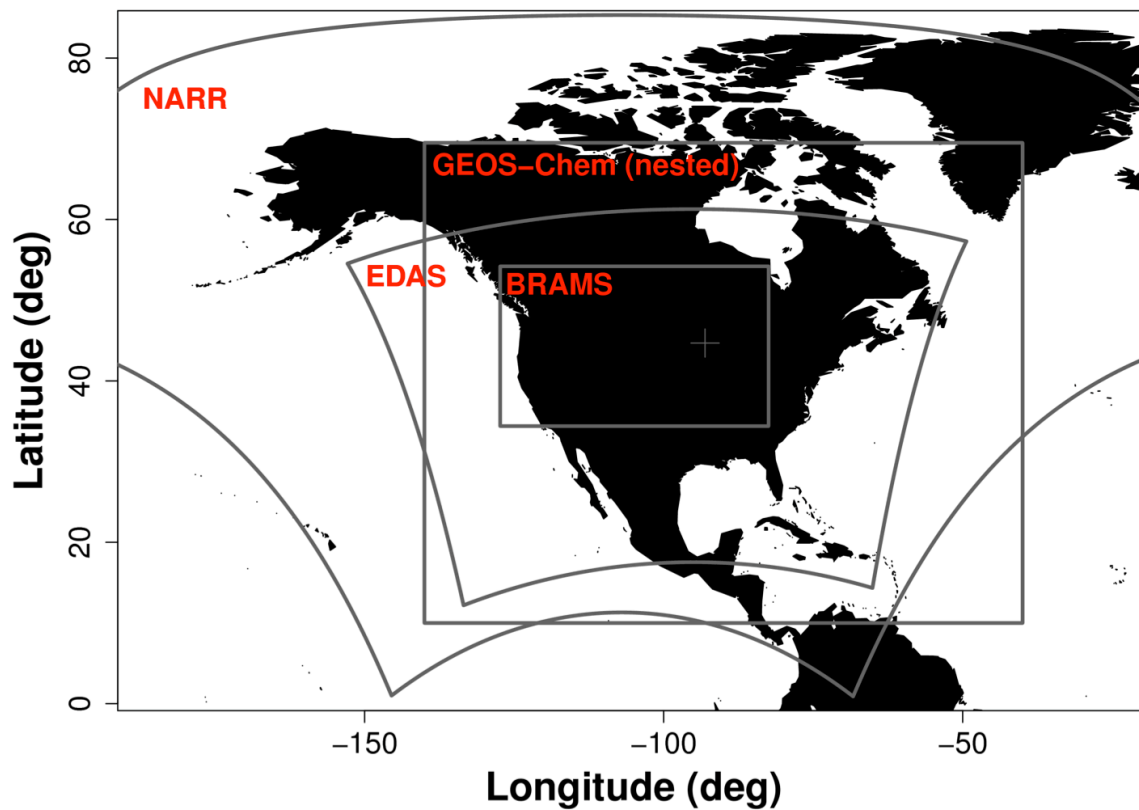
Figure S2. Spatial domains of the meteorological datasets used in this analysis. The location of the KCMP tall tower is indicated by the "+" symbol. GEOS-Chem was run over the domain shown for the nested 0.5° × 0.667° simulation, and globally for the 2° × 2.5° and 4° × 5° simulations.
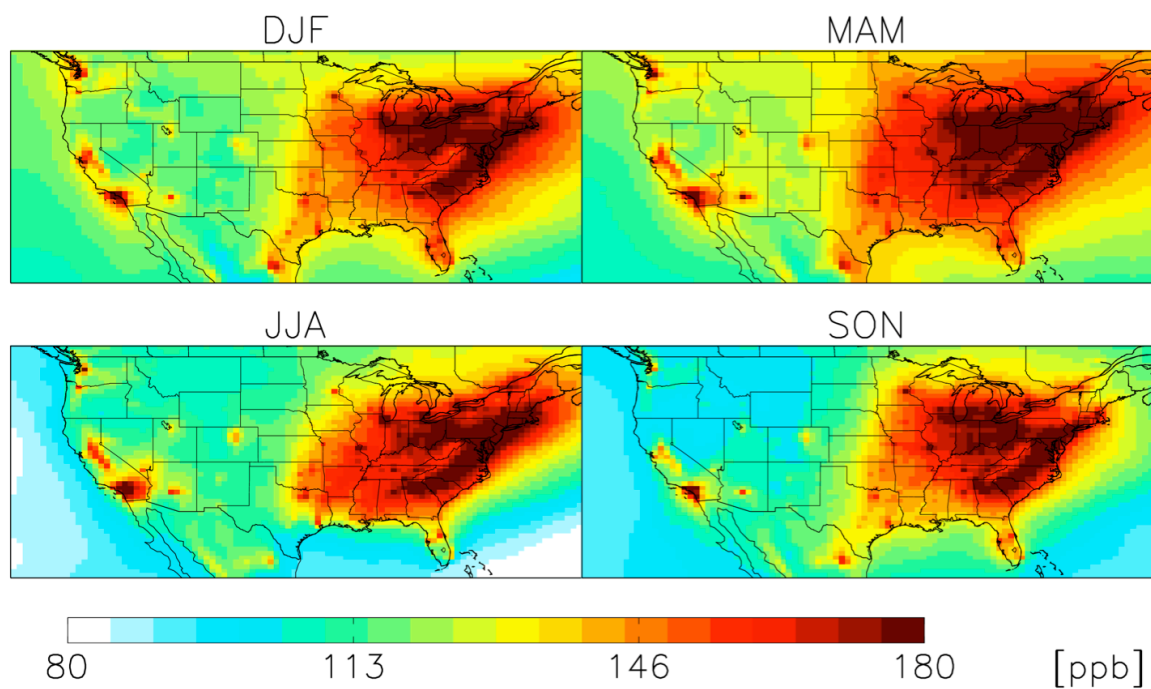
Figure S3. Seasonal boundary layer CO concentrations over North America as simulated by GEOS-Chem. Concentrations shown are boundary layer averages ($P > 800$ hPa) from the a priori nested $0.5° \times 0.667°$ simulation described in the main text. DJF = December, January, February; MAM = March, April, May; JJA = June, July, August; SON = September, October, November.
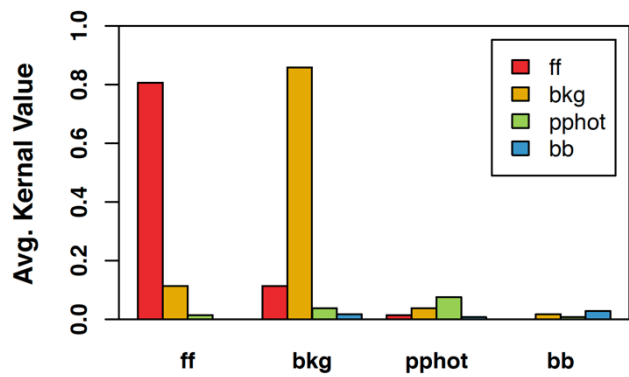
Figure S4. Averaging kernel for a CO optimization using EDAS meteorological fields (daytime + nighttime). ff: fossil fuel emissions; bkg: CO background; pphot: photochemical production; bb: biomass + biofuel burning.
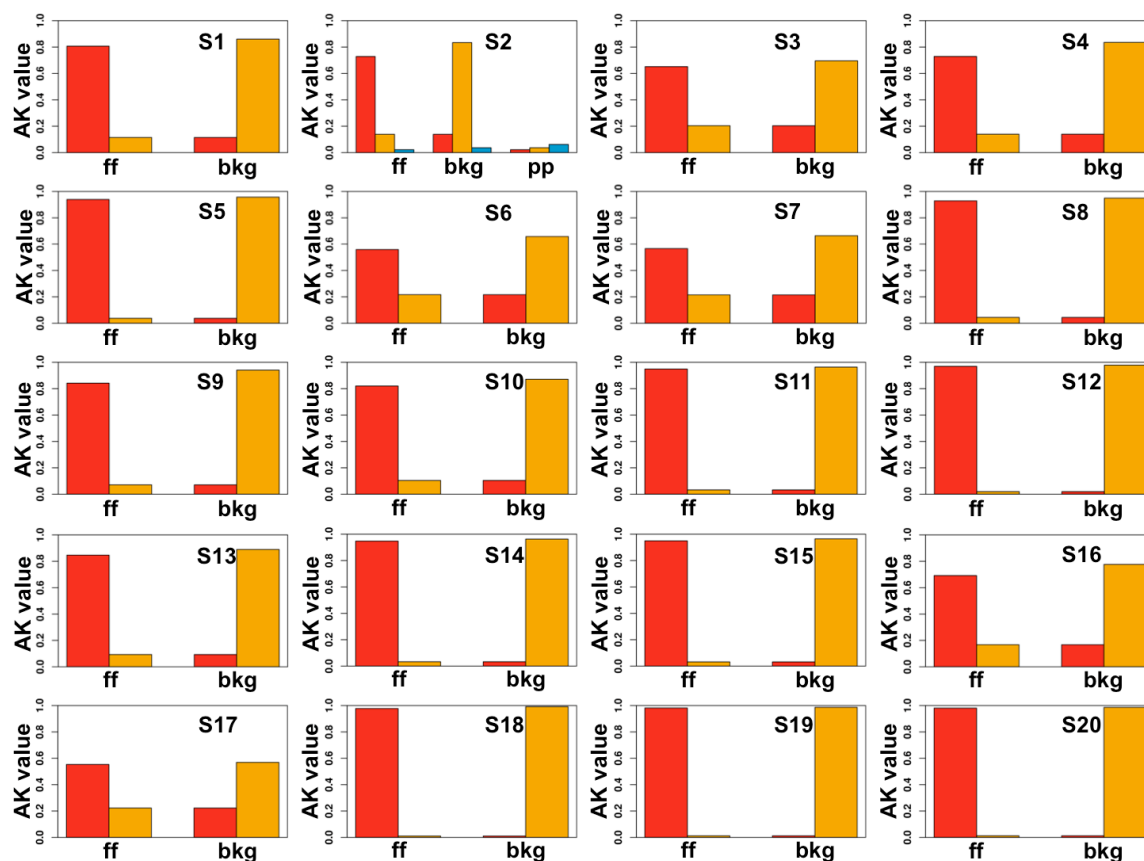
Figure S5. Averaging kernel for the best-estimate CO optimization (O1) and 19 additional sensitivity inversions (O2-O20; see Table 1 in the main text). ff: fossil fuel emissions; bkg: CO background; pp: photochemical production. Color scheme is as in Figure S4.
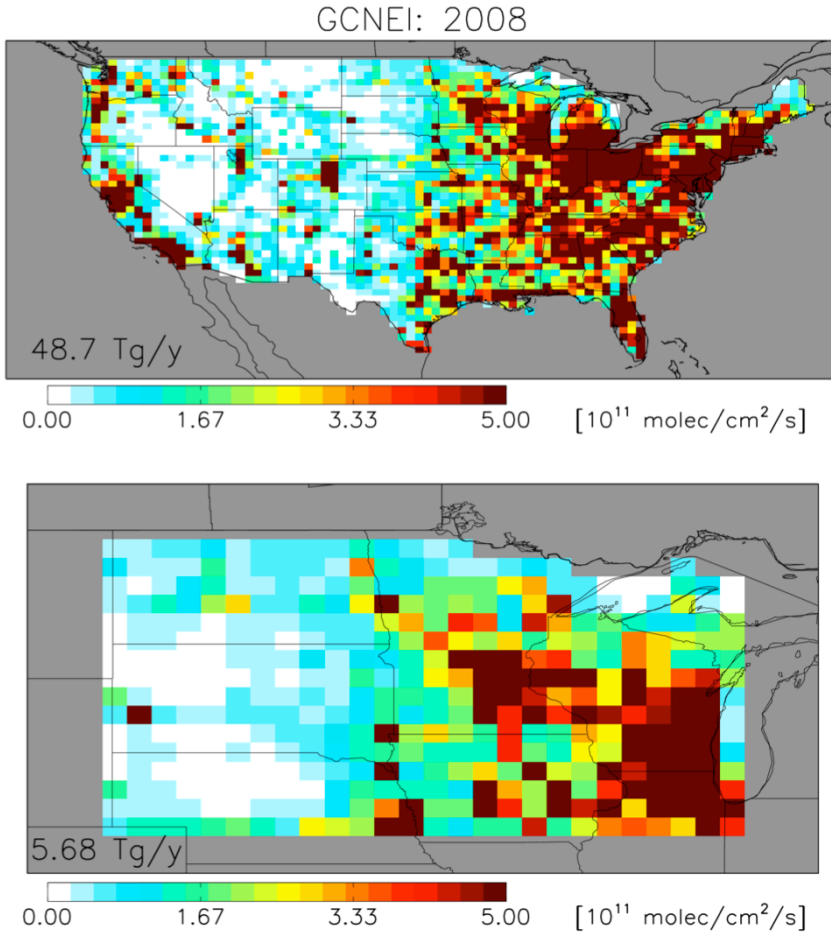
Figure S6. Annual anthropogenic surface CO emissions in the NEI 2008 emission inventory as implemented in GEOS-Chem at 0.5° × 0.667° resolution. Emissions shown are for year 2008 and do not include fires. Numbers inset give the annual flux for the region plotted.
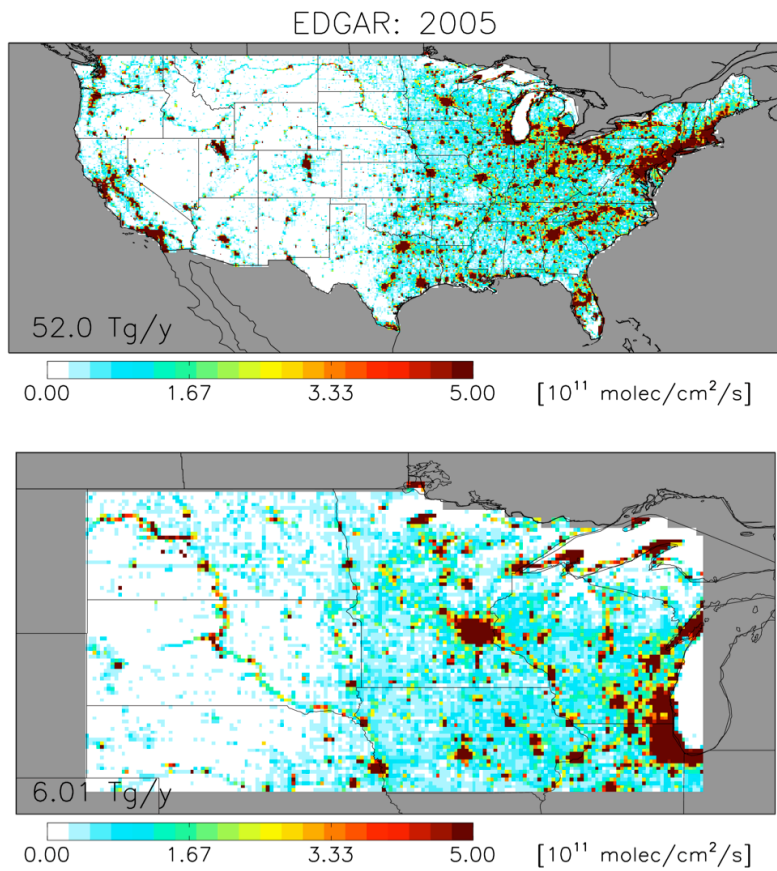
Figure S7. Annual anthropogenic surface CO emissions in the EDGARv4.2 emission inventory. Emissions are for year 2005 and gridded to 0.1° × 0.1°, and do not include fires. Numbers inset give the annual flux for the region plotted.
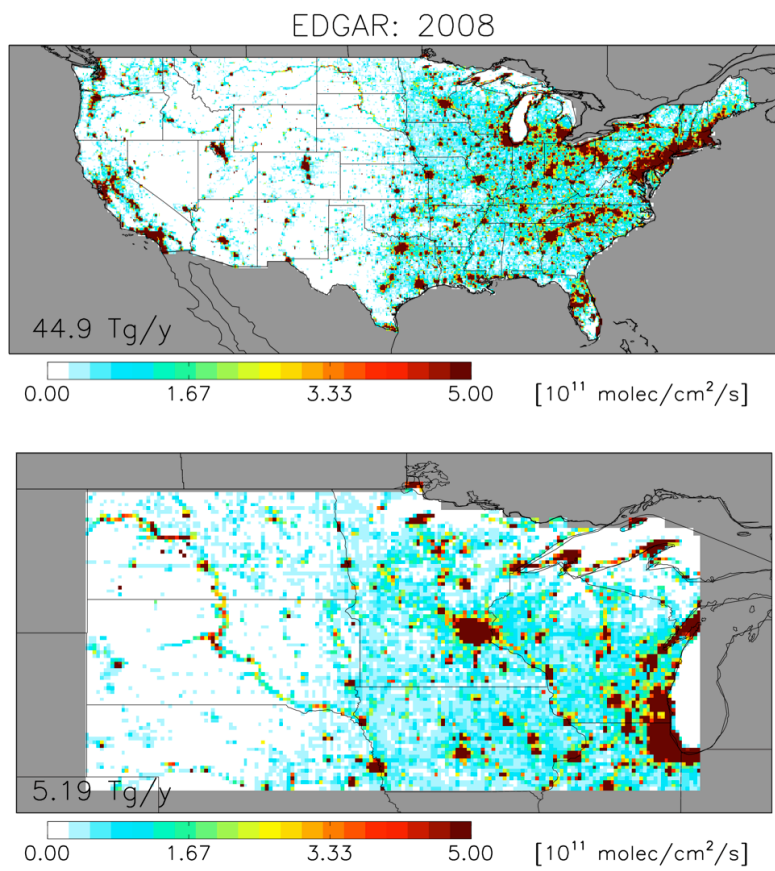
Figure S8. Annual anthropogenic surface CO emissions in the EDGARv4.2 emission inventory. Emissions are for year 2008 and gridded to 0.1° × 0.1°, and do not include fires. Numbers inset give the annual flux for the region plotted.